S5A). Hence, p53 phosphorylation in Ser[9] and Ser[6] serves as integration node in the cross-talk between Ras/MAPK and TGF-β.

This prompted us to consider the possibility that, although p53 is a ubiquitous protein, FGF might spatially pattern p53's activity. In *Xenopus*, expression of different FGFs (eFGF, FGF3, and FGF8) is enriched in the marginal zone of the embryo, from which the mesoderm emerges, whereas lower FGF activity is present in the animal pole (*10*) (Fig. 3A). Using phosphospecific antibodies, we found that kinase activities targeting Ser[9] and Ser[6] are localized in the marginal zone; in contrast, phosphorylation in other residues appears constitutive (Fig. 3B). To determine whether endogenous FGF signaling is responsible for this graded p53 phosphorylation along the animal-vegetal axis, embryos were treated with the FGF-receptor inhibitor SU5402 or injected with *DN-Raf*˙ mRNA. Blockade of FGF signaling causes specific down-regulation of P-Ser[9] and P-Ser[6] (Fig. 3C). Conversely, ectopic FGF expression in animal cap cells specifically raises P-Ser[6] and P-Ser[9] levels (Fig. 3D). Similarly, at the biochemical level, FGF is required for p53/Smad2 interaction because the formation of this complex is inhibited by SU5402 (fig. S6). However, introduction of Ser to Glu phosphomimicking substitutions in Ser[6] and Ser[9] (p53S6,9E), renders p53 able to complex with Smad2 in an FGF-independent manner (fig. S6). Together, the results indicate that FGF patterns the phosphorylation status of p53 in the embryo, restricting its cooperation with TGF-β to the prospective mesoderm.

Next, we wished to gain insight into the kinase responsible for inducing p53 phosphorylation in response to FGF/Ras/MAPK signaling. Both Ser[6] and Ser[9] conform to a CK1 consensus: There are seven mammalian CK1 genes, but p53 has been shown to associate specifically with CK1ε and CK1δ (*11*). In *Xenopus* embryos, inhibition of these kinases with dominant-negative CK1ε (DN-CK1ε) (*12*, *13*) antagonizes FGF-mediated Ser[6] and Ser[9] phosphorylation (fig. S7). Biologically, increasing levels of CK1ε promote mesoderm induction in a p53-dependent manner (Fig. 3E and fig. S8); conversely, loss-of-CK1ε by microinjection of DN-CK1ε or CK1ε morpholino inhibits endogenous and p53-mediated mesodermal gene expression (Fig. 3, F and G, and fig. S9). Thus, CK1ε lies downstream of FGF to promote p53 phosphorylation and Smad cooperation in *Xenopus* mesoderm development.

We next investigated the relevance of CK1ε/δ-mediated p53 phosphorylation on the activation of the TGF-β cytostatic program in human cells. To this end, p53-reconstituted H1299 cells were transfected with siRNAs to deplete endogenous CK1ε and CK1δ. CK1ε/δ knockdown leads to down-regulation of P-Ser[6] and P-Ser[9] levels (Fig. 3H) and to loss of TGF-β–mediated p21[Waf1] induction (Fig. 3I, compare phosphomimicking substitution of Ser[9] with Glu (p53S9E) renders p53 able to sustain TGF-β–mediated p21[Waf1] induction even in the absence of CK1ε/δ (Fig. 3I, compare lane 4 with lane 8 and lane 6 with lane 10). Hence, p53S9E acts epistatically to CK1ε/δ. This indicates the key role of p53 N-terminal phosphorylation as mediator of the positive effect of CK1ε/δ in supporting TGF-β cytostatic responses.

We have established a role for p53 as signaling integrator, outside of its widely investigated response to genotoxic stress (*8*). We provide evidence that p53 activity, rather than stability, can be qualitatively patterned by RTK/Ras-induced phosphorylation through CK1ε/δ. This phosphorylation step enables a robust biochemical interaction of p53 with TGF-β–activated Smads, leading to mesoderm induction in embryos and, in human cells, to the deployment of the TGF-β cytostatic program.

These data establish a mechanistic link between three key regulators of cell proliferation that are dysregulated in human cancers: Ras, p53, and TGF-β. This could provide an explanation for the p53-dependent tumor-suppressive function of Ras/MAPK reported in primary cells (*14*, *15*). Activated Ras may well have general growth-promoting effects but, in the presence of wild-type p53, this would be balanced by the positive role played on p53/Smad cooperation that would sustain TGF-β growth control and thus limit neoplastic transformation.

**References and Notes**

1. L. Attisano, J. L. Wrana, *Science* **296**, 1646 (2002).
2. J. Schlessinger, *Cell* **103**, 211 (2000).
3. C. LaBonne, M. Whitman, *Development* **120**, 463 (1994).
4. R. A. Cornell, D. Kimelman, *Development* **120**, 453 (1994).
5. P. P. Hu *et al.*, *J. Biol. Chem.* **274**, 35381 (1999).
6. R. T. Bottcher, C. Niehrs, *Endocr. Rev.* **26**, 63 (2005).
7. M. Cordenonsi *et al.*, *Cell* **113**, 301 (2003).
8. A. M. Bode, Z. Dong, *Nat. Rev. Cancer* **4**, 793 (2004).
9. T. Mitsudomi *et al.*, *Oncogene* **7**, 171 (1992).
10. C. LaBonne, B. Burke, M. Whitman, *Development* **121**, 1475 (1995).
11. U. Knippschild *et al.*, *Oncogene* **15**, 1727 (1997).
12. X. Zeng *et al.*, *Nature* **438**, 873 (2005).
13. G. Davidson *et al.*, *Nature* **438**, 867 (2005).
14. S. W. Lowe, E. Cepero, G. Evan, *Nature* **432**, 307 (2004).
15. E. Roper, W. Weinberg, F. M. Watt, H. Land, *EMBO Rep.* **2**, 145 (2001).
16. We thank G. Bressan and D. Volpin for discussion. We also thank G. Del Sal, M. Mechali, D. Lane, C. Niehrs, J. Graff, D. Morrison, and K. Vousden for gifts of plasmids or antibodies, G. Blandino for the gift of p53-reconstituted cells, and O. Wessely for comments. This work is supported by grants to S.P. from Associazione Italiana per la Ricerca Sul Cancro, TELETHON-Italy GGP04030, MIUR (CoFin, FIRB), Agenzia Spaziale Italiana, Istituto Superiore di Sanita, and Swissbridge. A.M. is recipient of a European Union Marie Curie Research Training Network fellowship (Epiplast Carcinoma). M.C. was supported by a FIRC fellowship.

**Supporting Online Material**

www.sciencemag.org/cgi/content/full/1135961/DC1
Materials and Methods
Figs. S1 to S9
References

5 October 2006; accepted 22 December 2006
Published online 18 January 2007;
10.1126/science.1135961
Include this information when citing this paper.

# Structure of the Prefusion Form of the Vesicular Stomatitis Virus Glycoprotein G

**Stéphane Roche, Félix A. Rey,* Yves Gaudin,† Stéphane Bressanelli**

**Glycoprotein G of the vesicular stomatitis virus triggers membrane fusion via a low pH–induced structural rearrangement. Despite the equilibrium between the pre- and postfusion states, the structure of the prefusion form, determined to 3.0 angstrom resolution, shows that the fusogenic transition entails an extensive structural reorganization of G. Comparison with the structure of the postfusion form suggests a pathway for the conformational change. In the prefusion form, G has the shape of a tripod with the fusion loops exposed, which point toward the viral membrane, and with the antigenic sites located at the distal end of the molecule. A large number of G glycoproteins, perhaps organized as in the crystals, act cooperatively to induce membrane merging.**

The Rhabdoviridae are enveloped bullet-shaped viruses that are widespread among a great variety of organisms, including plants, insects, fishes, mammals, reptiles, and crustaceans (*1*). This family includes vesicular stomatitis virus (VSV) as well as notable human pathogens, such as rabies virus (RV) and Chandipura virus (*2*).

The rhabdoviruses enter the cell via the endocytic pathway and subsequently fuse with a cellular membrane within the acidic environment of the endosome (*3*). Both receptor recognition and membrane fusion are mediated by a single transmembrane (TM) viral glycoprotein (G) that is trimeric and forms the spikes that

CNRS, Unité Mixte de Recherche (UMR) 2472, Institut National de la Recherche Agronomique (INRA), UMR 1157, Institut Fédératif de Recherche 115, Laboratoire de Virologie Moléculaire et Structurale, 91198, Gif sur Yvette, France.

*Present address: Département de Virologie, Institut Pasteur, 25 rue du Docteur Roux, 75724 Paris cedex 15, France.
†To whom correspondence should be addressed. E-mail:

domain of G (446 out of 495 amino acids for the VSV Indiana strain) is also the target of neutralizing antibodies, and the antigenic sites of G in both VSV and RV have been described in detail (*4*–*6*).

Similar to other viral fusion proteins, G undergoes a fusogenic structural transition during cell entry (*7*, *8*). As for influenza virus hemagglutinin (HA), flavivirus E protein, and Semliki Forest virus E1 protein, the conformational change is triggered at low pH (*9*). G can adopt at least three conformational states (*7*, *8*, *10*–*14*): the native prefusion state detected at the viral surface above pH 7; the activated hydrophobic state, which interacts with the membrane as a first step of the fusion process (*11*); and the fusion-inactive postfusion conformation that is antigenically distinct from both the native and activated states. There is a pH-dependent equilibrium between the different states of G that is shifted toward the postfusion conformation at low pH (*15*). Thus, unlike fusogenic proteins from other viral families, the native prefusion conformation is not metastable (*9*). Indeed, the reversibility of the low pH–induced conformational change is essential to allow G to be transported through the acidic compartments of the Golgi apparatus and to recover its native functional state at the viral surface (*16*).

We have recently determined the low-pH postfusion three-dimensional structure of the VSV G ectodomain (residues 1 to 422), generated by limited proteolysis of the virions with thermolysin ($G_{th}$) (*17*). In spite of having an unrecognized fold distinct from those of other fusion proteins previously described, the postfusion conformation of G displays the classic hairpin conformation of other viral fusogenic proteins [i.e., an elongated structure with the fusion domain and the TM domain at the same end of the molecule (*18*)]. As in class I fusion proteins (*19*–*21*), the postfusion trimer displays a six-helix bundle with the fusion domains at the N terminus of the central helices and the TM domains at the C terminus of the antiparallel outer helices. Each fusion domain bears two fusion loops located at the tip of an elongated β sheet, which is a marked convergence with class II fusion proteins (*22*–*24*). Unexpectedly, G turned out to be homologous to glycoprotein gB of herpesviruses, the atomic structure of which was published at the same time (*25*). Because the low pH–induced conformational change of rhabdoviral G is reversible, it remained unclear to what extent the pre- and postfusion conformations differed for this class of fusion proteins.

Among the different crystal forms obtained with $G_{th}$ (*17*) (see also the materials and methods in the supporting online material), one of them, which was grown at pH 8.7, appeared to be particularly notable, because the asymmetric unit could not accommodate the postfusion form (125 Å in length) but was consistent with the presence of one protomer of the prefusion form [8.5 nm in length as measured for the RV G ectodomain by electron microscopy (EM) (*26*)]. This crystal structure of $G_{th}$ was determined to 3.0 Å resolution by molecular replacement with the use of domains I, III, and IV (Table 1) of the low-pH form as search models. Data collection and refinement statistics are given in table S1. The structure of $G_{th}$ is depicted in Fig. 1. Its length (88 Å), the location of the antigenic sites, and the comparison with the low-pH structure indicate that this $G_{th}$ structure corresponds to the prefusion conformation of the molecule. The chain can be traced up to residue 413 (see the electron density for the final model in fig. S1). Clear density is also present for the first residues of both oligosaccharide chains (on $N^{163}$ and $N^{320}$) (*27*), which were disordered in the structure of the low-pH form.

**Table 1.** Domain nomenclature used in the text. Root mean square deviation (RMSD) is between the pre- and postfusion structures. The number of alpha carbons (Cα) used in superposing the domains is indicated in parentheses.

| Domain | Domain name | Color | Residues | RMSD |
|---|---|---|---|---|
| DI | Lateral domain | Red | 1 to 17 and 310 to 382 | 0.42 Å (80 Cα) |
| DII | Trimerization domain | Blue | 18 to 35, 259 to 309, and 383 to 405 | - |
| DIII | PH domain | Orange | 36 to 46 and 181 to 258 | 0.40 Å (82 Cα) |
| DIV | Fusion domain | Yellow | 53 to 172 | 0.77 Å (94 Cα) |
| Cter | C-terminal part | Magenta | 406 to 413 | - |
| RbI-II | Rigid block | - | 1 to 25 and 273 to 382 | 0.56 Å (122 Cα) |

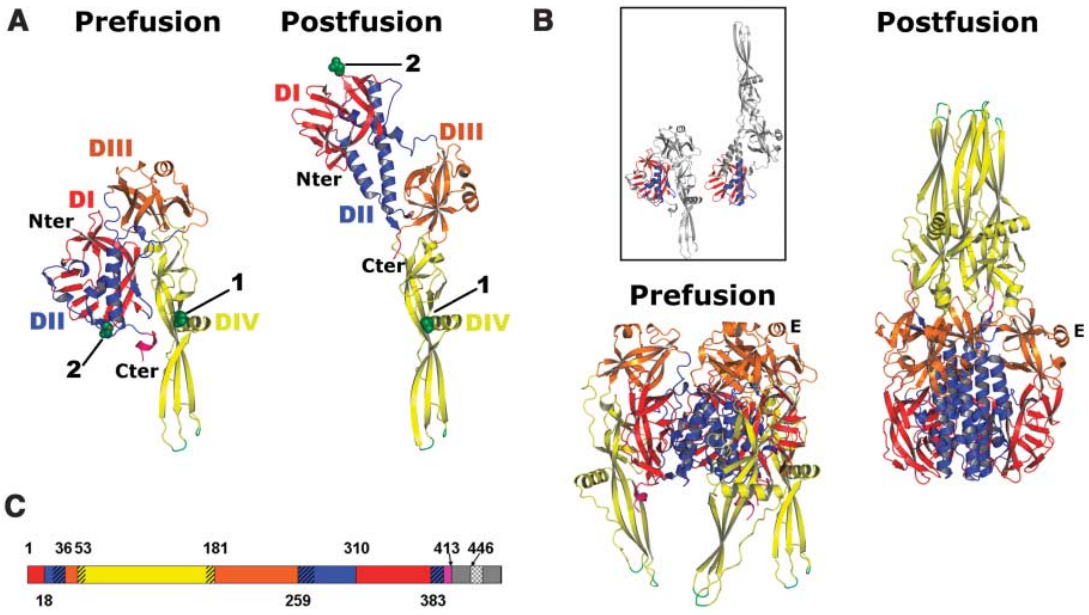


**Fig. 1.** Overall $G_{th}$ structure in pre- and postfusion conformations. (**A**) View of the G protomers superimposed on their fusion domains (DIV) and colored by domain (as defined in Table 1) with the fusion loops in green. The two glycosylated asparagines [$N^{163}$ (labeled "1") and $N^{320}$ (labeled "2")] are displayed as dark green spheres. (**B**) View of the G trimers, colored by domains as in (A). The trimers were superimposed on the rigid blocks made of DI and the invariant part of DII (RbI-II, defined in Table 1 and highlighted in the boxed inset for one protomer of each conformation). Helix E is indicated on both trimers. (**C**) Domain architecture of VSV G plotted on a linear diagram, color-coded according segment is in gray, with a checkerboard pattern for the TM domain. The regions that refold in the transition are hatched. All structural figures were

The overall architecture of $G_{th}$ in its prefusion state resembles a tripod (Fig. 1B). Each leg is composed of a fusion domain with the fusion loops pointing toward the viral membrane. The last residues that we can see (including the conserved $H^{407}$ and $P^{408}$) pack against the side of the fusion domain. This organization, which is reminiscent of the low-resolution structure of retroviruses' envelope spikes that was recently determined by EM (*28*, *29*), suggests that the TM segments are separate in the membrane. Nevertheless, we cannot exclude the possibility that the missing C-terminal segments of the ectodomain (residues 414 to 446) that lead to the TM segments come together toward the threefold axis.

In the tripod arrangement, the fusion domains are set wide apart, keeping the fusion loops separate (Fig. 1B, left). In contrast to class I and class II fusion proteins, the fusion loops of G are not buried at an oligomeric interface in the prefusion conformation. The hydrophobic residues $Y^{116}$, $A^{117}$, $W^{72}$, and $Y^{73}$ are exposed (Fig. 1, A and B), even though they cluster near crystal contacts (fig. S3D). The tips of the fusion domains are the most flexible part of the structure (fig. S4) and thus are the least well defined in the electron density maps.

The conformational change involves a dramatic reorganization of the G molecule. Figure S2 shows a comparison of the secondary structure elements of the two conformations with their nomenclature. The pre- and postfusion states are related by flipping both the fusion domain and a C-terminal segment (composed of residues 383 to 413) relative to a rigid block (RbI-II) made by the lateral domain and residues of the trimerization domain that include helix F2 of the prefusion form (Table 1 and Fig. 1B, inset). During the structural transition, both the fusion loops and the TM domain move ~160 Å from one end of the molecule to the other. Thus, the observed conformational change, although reversible, appears to be similar to that of paramyxovirus F glycoprotein (*30*). It also suggests that similar intermediates are formed during the fusion-associated refolding of G, HA, and paramyxovirus F glycoprotein (*19*, *30*). In one of these intermediates (Fig. 2C and movie S1), the fusion domain is projected at the top of the spike, allowing the initial interaction with the target membrane.

In spite of large rearrangements in their relative orientation (Fig. 2, A and B), domains I, III, and IV retain their folded structure (Table 1 and Figs. 1A and 2). In this and the following paragraphs, we describe the conformational change of a protomer by considering RbI-II as invariant (Fig. 1B, inset). The flippings of both the fusion domain and the TM segment relative to RbI-II occur through a concerted rearrangement of distinct regions of the molecule. Although we have only snapshots of the initial and final states, analysis of the two structures (see the description of movie S1 in the supporting online material) suggests a plausible sequence of events leading from pre- to postfusion conformations.

The fusion domain is projected toward the target membrane through the combination of two movements (Fig. 2C): a 94° rotation around the hinge between the fusion and pleckstrin homology (PH) domains (Fig. 2A) and the repositioning of the latter domain at the top of the trimerization domain (Fig. 2B). The rotation involves the reorganization of two segments (residues 47 to 52 and 173 to 180) of the polypeptide chain. In the former segment, helix $A^0$ unfolds whereas, in the latter segment, helix C forms (Fig. 2A). Mutations $M^{44} \longrightarrow$ V or I in RV G, which kinetically stabilize the native conformation (*31*), map to this region. Their location suggests that they impede the slight distortion of strands b and j of the PH domain that accompanies the movement.

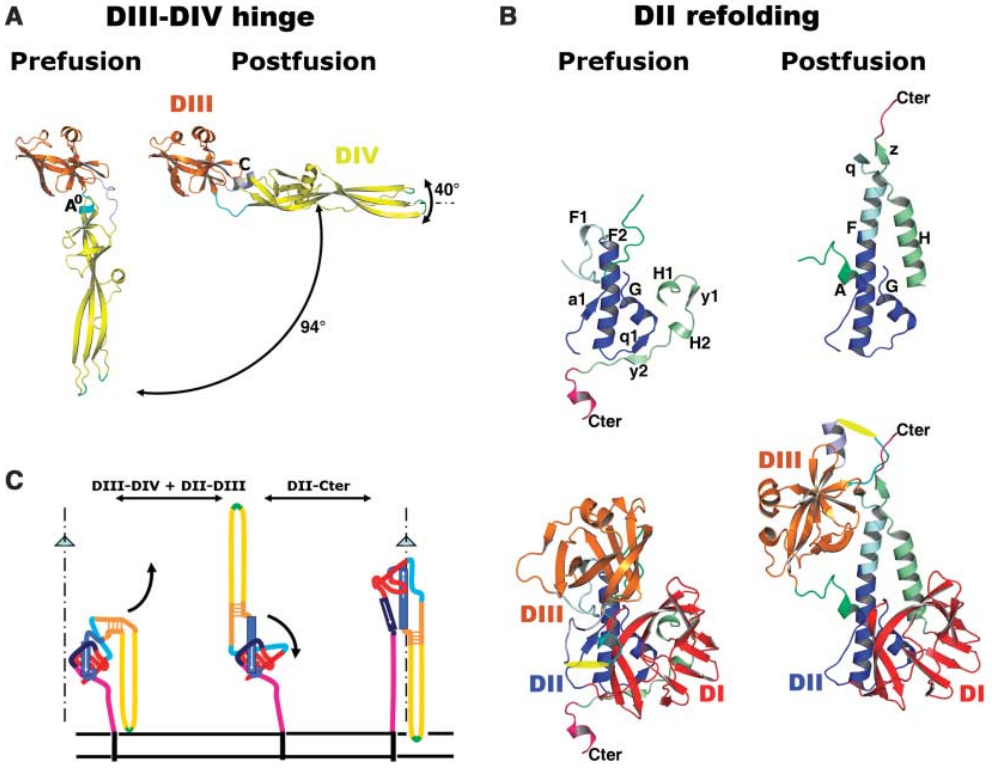


**Fig. 2.** Structural changes in the protomer between the pre- and postfusion conformations and relative movements of domains. In (A) and (B), fragments of the pre- and postfusion conformations are displayed to the left and right, respectively. Secondary structure elements of the prefusion form that refold are named and numbered according to fig. S2. (**A**) Relative movement of PH (DIII, orange) and fusion (DIV, yellow) domains. The protomers are superimposed on DIII. Hinge residues 47 to 52 (prefusion helix $A^0$) and 173 to 180 (postfusion helix C) are colored in cyan and gray-blue, respectively. (**B**) Domain II refolding. DI and DIII are omitted in the top panels for clarity but are shown in the bottom panels to provide the relative orientations in the two forms. The protomers are superimposed on the invariant part of DII, which is indicated in dark blue, whereas the three segments that refold and/or relocate are indicated in shades of green. In the prefusion form, strands $a^1$ and $y^1$ form an interchain β sheet. The DIII-DIV hinge (bottom panels) is displayed and colored as in (A), with the two segments connected by a yellow bar to mark the location of the fusion domain. (**C**) Cartoon representation of the relative organization of domains with respect to the viral membrane during the conformational change. The one-sided black arrows indicate the (blue; left), F (blue; middle and right), and H (dark blue; right) are indicated with white arrows. Pre- (left) and postfusion (right) conformations are shown. The trimer axes are indicated. The middle cartoon shows how the fusion loops (in green) would be projected after the refolding of both the DIII-DIV hinge and

The trimerization domain undergoes a major refolding event during the transition between the pre- and postfusion structures (Fig. 2B). This refolding drives the repositioning of the PH domain and the flipping of the C-terminal part and involves all three segments of the trimerization domain (Fig. 1C).

As a first step, central helix F2 (residues 276 to 294) is lengthened by the recruitment of a segment (made up of residues 263 to 275) to form the long helix F. The second segment that refolds is composed of residues 26 to 35, which, in the prefusion conformation, is buried in a groove of RbI-II that is closed by residues 263 to 275. A sharp bend is introduced right after the conserved motif $C^{24}P^{25}$: The peptide bond between $P^{25}$ and $S^{26}$ flips, which redirects the polypeptide chain at an 80° angle, and short helix A (residues 24 to 29) is formed. The conformation of short strand $a^1$ (residues 22 to 24), involved in the interchain β-sheet $a^1y^1$ in the prefusion conformation, is unchanged, although it is not paired to strand $y^1$ of the adjacent protomer in the postfusion conformation (Fig. 2B).

The small β-sheet $q^1y^2$ of the native form is then broken, although the individual strands $q^1$ and $y^2$ retain their β conformation in the postfusion form, and residues 384 to 400 (including helices H1 and H2 and strand $y^1$) refold into helix H. This helix then positions itself in the grooves of the central core in an antiparallel manner to form the six-helix bundle. This movement repositions the TM domains at the same end of the molecule as the fusion domains (Figs. 1B and 2B). Finally, residues 259 to 261 and 403 to 405, which are distant by ~30 Å in the prefusion conformation, form sheet qz that zips together helices F and H in the postfusion state (Fig. 2B). Strands q and z are already in an extended β structure in the native conformation, primed to form sheet qz in the postfusion form.

The buried interface between two subunits in the trimer is 1600 $Å^2$ per protomer, as calculated by the Protein Interfaces, Surfaces, and Assemblies server (*32*). This value is less than half of that of the buried interface in the low-pH form. This explains the increased stability of the oligomeric structure of G at low pH (*8*). The interactions between protomers are all located in domain II (fig. S5) but are different from those observed in the postfusion form (Fig. 3, A and B). Not only is prefusion helix F2 shorter than postfusion helix F, it is also tilted and its C-terminal end is kept away from the trimer axis (Fig. 3A). This results from repulsive forces between the carboxylates of the three $E^{286}$ amino acids (Fig. 3C). In contrast to the postfusion form, the main contribution to trimer stability is not due to the central helix bundle but appears to come from interchain β-sheet $a^1y^1$ [which must break during the fusogenic transition, before the formation of helix H (Fig. 2B)] and its environment, burying 1250 $Å^2$ per protomer (Fig. 3D). The surface even in absence of the target membrane. This seems to be topologically impossible without transient dissociation of the trimer. This hypothesis is in agreement with the large differences in the trimeric interfaces between the native and the postfusion conformations of G.

A number of the few conserved residues (fig. S2) are involved in key networks of interactions that are different in the two forms (Fig. 4). This set of residues includes amino acids $D^{137}$, $Y^{139}$, $H^{407}$, and $P^{408}$ that cluster together in the postfusion conformation to stabilize β-sheet qz of the trimerization domain (Fig. 4B). In the prefusion conformation, the qz sheet does not exist: $D^{137}$ and $Y^{139}$ remain associated with the segment corresponding to the q strand and contribute to a network of hydrogen bonds that also involves conserved $W^{236}$ of the PH domain (Fig. 4A, top). This network is disorganized during the rotation of the fusion domain relative to the PH domain (Fig. 2A). Conserved histidines—$H^{407}$ [involved in a salt bridge with $D^{137}$ in the low-pH structure (Fig. 4B)], $H^{162}$ [previously shown to be involved in the interactions between fusion do-

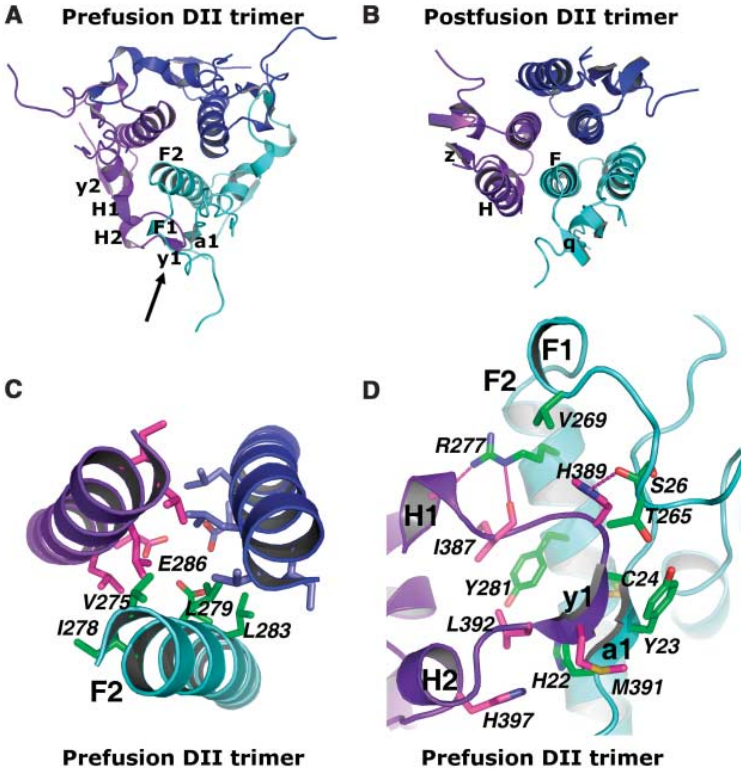


**Fig. 3.** The trimeric interface of the prefusion conformation [(A), (C), and (D)] as compared to that of the postfusion conformation (B). For clarity, only DII [the only domain involved in the interface in the prefusion conformation (fig. S5)] is represented, and the three protomers are colored in three shades of blue. Secondary structure elements that refold and/or relocate are labeled. (**A**) Top view (orientation as in fig. S5, looking down toward the viral membrane) of the trimeric interface of the prefusion conformation. The arrow indicates the viewpoint used in (D). (**B**) Trimeric interface of the postfusion conformation, superimposed on the invariant parts of DII in (A). The view therefore would now be from the membrane. (**C**) Zoom of image in (A) showing only the three helices F2 and the side chains involved in their interactions, which are colored by atom type (oxygen, red; nitrogen, blue; sulfur, yellow; carbon: green, magenta, or dark blue, depending on the protomer) and labeled. As in the postfusion state, $V^{275}$ and $L^{279}$ contribute to hydrophobic stabilizing interactions at the center of the molecule, but $L^{283}$ now makes a lateral interaction with $I^{278}$. The three $E^{286}$ amino acids in the center are 4 Å apart in native crystals. In the$YbCl_3$-derivative crystal used for refinement of the model (table S1), they chelate an ytterbium ion (not shown), bringing their side-chain oxygen atoms within 3.5 Å. (**D**) Close-up view of the outer region of the prefusion trimeric interface seen from the side. Contact residues are colored as in (C), with main-chain atoms included only when they participate in the contacts. Besides the canonical hydrogen bonds of the β sheet, the interface is stabilized through extended van der Waals contacts and a hydrogen bond between the imidazole ring and the carboxyl group of $T^{265}$ of the neighboring protomer. Finally, carboxyl groups of $L^{384}$ and $I^{387}$ make two hydrogen bonds with the guanidium group of $R^{277}$ of the other chain. These three hydrogen bonds are displayed as magenta

mains in the low-pH conformation (*17*)], and $H^{60}$—cluster together ($H^{60}$ is absent in RV G, but $H^{86}$, which corresponds to $S^{84}$ in VSV G, replaces it) (Fig. 4A, bottom). Protonation of these residues at low pH is likely to destabilize the interaction between the C-terminal segment of $G_{th}$ and the fusion domain in the prefusion conformation, priming the initial movement of the fusion domain toward the target membrane. Conversely, the acidic amino acids that were either buried at the trimer interface ($D^{268}$) or brought close together ($D^{274}$ with $D^{395}$ and $E^{276}$ with $D^{393}$) in the postfusion acidic conformation (*17*) are solvent-exposed in the prefusion state (not shown). Thus, the histidines in the prefusion form and the acidic residues in the postfusion form appear to constitute two pH-sensitive molecular switches.

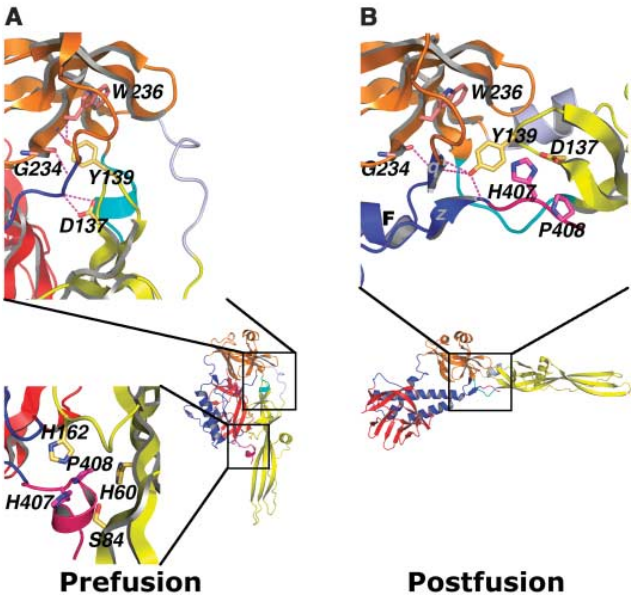


**Fig. 4.** Alternative networks of conserved residues in the pre- (**A**) and postfusion (**B**) conformations. The orientation is as that in Fig. 2A. Conserved residues are displayed in stick representation (main-chain atoms are not shown unless they participate in interdomain contacts). Hydrogen bonds are displayed as magenta dashed lines. [(A) and (B), top] Close-up views of the DIII-DIV connection are shown. The prefusion hydrogen bonds of $Y^{139}$ to the main chain of $W^{236}$ are relocated to the postfusion qz sheet, whereas $D^{137}$ switches from making a bidentate hydrogen bond to the main chain to engaging in a salt bridge with $H^{407}$. [(A), bottom] A close-up view of the prefusion DIV-Cter interface that has to be disrupted for DIV to move is shown. Note the cluster of conserved histidines, including $H^{407}$.

The major antigenic sites of rhabdoviruses are located in the lateral and PH domains (*4*–*6*) (Fig. 5). The accessibility of antigenic sites to antibodies has been studied in detail for RV G. Antibodies directed against RV G site II are unable to recognize the protein in its low-pH conformation (*7*, *15*). Indeed, during the structural transition, this site moves from the top of the molecule to a less accessible location at the surface of the virus. Conversely, the N-terminal epitope of RV G (NS) is only accessible in the low-pH conformation at the viral surface (*31*). Finally, RV G minor site a is recognized in both conformations (*7*). As for monoclonal antibody 17D2 (*33*) that binds only the prefusion conformation (*34*), its epitope is located in the segment of helix F that is unfolded in the native structure.

The cellular receptor of VSV G has not been identified. Nevertheless, a canyon located between the lateral and PH domains is exposed at the top of the molecule and could be involved in ligand binding (Fig. 5A). In support of this, residues 330 and 333 of RV G, which are involved in the recognition of the putative viral receptor p75 (low-affinity nerve growth factor receptor) (*35*) and which affect viral pathogenesis, align with residues 331 and 334 of VSV G, which are located at either end of the canyon.

In a previous study, we estimated the minimal number of trimeric spikes involved in the formation of a RV fusion complex as about 15 (*15*). At the viral surface, a local organization of the spikes resembling the P6 lattice found in the crystal (in which all the spikes are oriented identically, with the major antigenic sites exposed at their tops) (fig. S3) might organize the glycoproteins in an optimal manner for a concerted conformational change. It might also facilitate the formation of the initial intermediates on the fusion pathway. Indeed, the initial lipidic deformations leading to the formation of the stalk and the initial fusion pore (*36*) can form inside the inner rim of such a hexagon. Reinforcing the idea that the P6 organization may reflect the structure of a fusion relevant complex, a local hexagonal lattice of spikes of similar dimensions has been observed at low temperature under mildly acidic conditions at the surface of some RV G mutants that were affected in the kinetics of their low pH–induced structural transition (*31*).

It is often considered that fusogenic proteins drive membrane fusion by coupling irreversible protein refolding to membrane deformation (*37*). At least for rhabdoviral G, this is not the case. Rather, it appears that a concerted cooperative change of a large number of glycoproteins (perhaps organized in a hexagonal lattice, like the one present in the crystals) is used to overcome the high energetic barrier encountered dur-

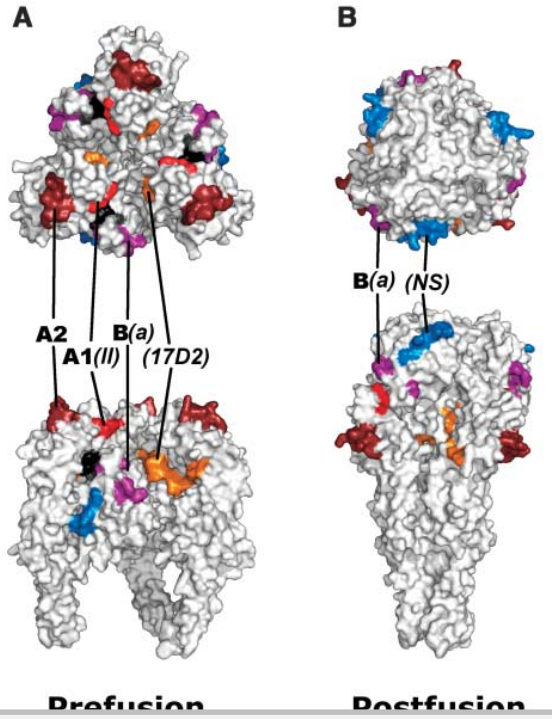


**Fig. 5.** Antigenic sites of Rhabdoviridae mapped onto the surface of the pre- (**A**) and postfusion (**B**) VSV G trimers. Sites are colored on both forms and labeled on the form(s) in which they are recognized. VSV sites are labeled in bold, and RV sites are labeled in italics within parentheses. VSV sites A1 (residues 37 to 38, corresponding to RV antigenic site II located on segments composed of residues 34 to 42 and 198 to 200) and A2 (located at the surface of helix E indicated in Fig. 1) are indicated in shades of red. The RV G site recognized by antibody 17D2 (between residues 255 and 270) is in orange. NS (extending from amino acid 10 to 15) is in dark blue. VSV site B (extending from amino acid 341 to 347), corresponding to RV G minor antigenic site a (amino acid 340 to 342), is in magenta. In the prefusion conformation, the cleft between DI and DIII is colored black. It is flanked by residues 331 and 334, in gray, whose counterparts in RV affect virulence.

DOCKET ALARM

# Explore Litigation Insights

Docket Alarm provides insights to develop a more informed litigation strategy and the peace of mind of knowing you're on top of things.

## Real-Time Litigation Alerts

Keep your litigation team up-to-date with **real-time alerts** and advanced team management tools built for the enterprise, all while greatly reducing PACER spend.

Our comprehensive service means we can handle Federal, State, and Administrative courts across the country.

## Advanced Docket Research

With over 230 million records, Docket Alarm's cloud-native docket research platform finds what other services can't. Coverage includes Federal, State, plus PTAB, TTAB, ITC and NLRB decisions, all in one place.

Identify arguments that have been successful in the past with full text, pinpoint searching. Link to case law cited within any court document via Fastcase.

## Analytics At Your Fingertips

Learn what happened the last time a particular judge, opposing counsel or company faced cases similar to yours.

Advanced out-of-the-box PTAB and TTAB analytics are always at your fingertips.

## API

Docket Alarm offers a powerful API (application programming interface) to developers that want to integrate case filings into their apps.

**LAW FIRMS**
Build custom dashboards for your attorneys and clients with live data direct from the court.

Automate many repetitive legal tasks like conflict checks, document management, and marketing.

**FINANCIAL INSTITUTIONS**
Litigation and bankruptcy checks for companies and debtors.

**E-DISCOVERY AND LEGAL VENDORS**
Sync your system to PACER to automate legal marketing.